Nuclear Structure Effects on Hyperfine Splittings in Ordinary and Muonic Deuterium

Chen Ji,[1,2,*] Xiang Zhang,[1] and Lucas Platter[3,4]

[1]*Key Laboratory of Quark and Lepton Physics, Institute of Particle Physics, Central China Normal University, Wuhan 430079, China*
[2]*Southern Center for Nuclear-Science Theory, Institute of Modern Physics, Chinese Academy of Sciences, Huizhou 516000, China*
[3]*Department of Physics and Astronomy, University of Tennessee, Knoxville, Tennessee 37996, USA*
[4]*Physics Division, Oak Ridge National Laboratory, Oak Ridge, Tennessee 37831, USA*

(Received 1 December 2023; revised 16 May 2024; accepted 21 June 2024; published 25 July 2024)

Precision spectroscopy of hyperfine splitting (HFS) is a crucial tool for investigating the structure of nuclei and testing quantum electrodynamics. However, accurate theoretical predictions are hindered by two-photon exchange (TPE) effects. We propose a novel formalism that accounts for nuclear excitations and recoil in TPE, providing a model-independent description of TPE effects on HFS in light ordinary and muonic atoms. Combining our formalism with pionless effective field theory at next-to-next-to-leading order, the predicted TPE effects on HFS are 41.7(4.4) kHz and 0.117(13) meV for the 1S state in deuterium and the 2S state in muonic deuterium. These results align within 1σ and 1.3σ from recent measurements and highlight the importance of nuclear structure effects on HFS and indicate the value of more precise measurements in future experiments.

DOI: 10.1103/PhysRevLett.133.042502

Introduction—Precision laser spectroscopy of atomic transitions informs on the structure of nuclei and tests the accuracy of bound-state quantum electrodynamics (QED). Measurements of Lamb shifts in light, muonic atoms have provided nuclear charge radii at unprecedented accuracy
[1–5]. In these experiments, a solid understanding of nuclear structure effects is crucial [6–13].

High-precision spectroscopy measurements of hyperfine splitting (HFS) have provided valuable insights into the nuclear magnetic structure. These measurements have been or will be conducted on light ordinary atoms such as ^{1,2}H, ^{3}He, and ^{6,7}Li [14–19], as well as their muonic atom counterparts [2–4,20,21]. HFS, predominantly governed by the short-range interaction between the nuclear and lepton magnetic moments [22–24], offers an ideal probe for studying the elastic and inelastic structure of nucleons and nuclei.

Accurate theoretical predictions for HFS in both ordinary and muonic atoms are limited by nuclear structure effects, entering through two-photon exchange (TPE). The elastic TPE, encoded in the "Zemach radius" r_Z, arises from the convolution of the nuclear charge and magnetic densities [25,26]. The inelastic TPE, namely the nuclear polarizability, stems from nuclear virtual excitations.

For ^{2}H and μ^2H, the discrepancy between the measured HFS and the calculated QED contribution for the 1S state of ^{2}H is [15,24]

$$\nu_{\rm exp}(^2{\rm H}) - \nu_{\rm QED}(^2{\rm H}) = 45.2\ {\rm kHz}, \tag{1}$$

and for the 2S state of μ^2H is [27,28]

$$\nu_{\rm exp}(\mu^2{\rm H}) - \nu_{\rm QED}(\mu^2{\rm H}) = 0.0966(73)\ {\rm meV}. \tag{2}$$

These discrepancies mainly arise from TPE. However, an accurate, uncertainty-quantified, and model-independent prediction of the TPE effect on HFS has not been achieved yet [28–33]. For instance, the conventional Low-term formalism inadequately accounts for nuclear excitations, thus providing an incomplete description [30,31].

This Letter introduces a new formalism for the TPE effect on HFS that accurately incorporates nuclear excitations and recoil. Using pionless effective field theory ($\not\pi$EFT) at next-to-next-to-leading order (NNLO), we then evaluate TPE contributions in ^{2}H and μ^2H. The formalism offers a model-independent description of the TPE effect with systematic uncertainty quantification, showing consistency with $\nu_{\rm exp}$-$\nu_{\rm QED}$ in ^{2}H and μ^2H.

Two-photon exchange theory—HFS of $ns_{1/2}$ states is dominated by contact interactions between the lepton spin $\boldsymbol{\sigma}_\ell/2$ and the nuclear spin $\boldsymbol{I}$ [22–24]

$$\mathcal{H}_I = \frac{2\pi\alpha g_m}{3m_\ell m_N}\phi_n^2(0)\boldsymbol{\sigma}^{(\ell)}\cdot\boldsymbol{I}, \tag{3}$$

where α is the electromagnetic fine structure constant, g_m denotes the nuclear magnetic g factor, and m_ℓ (m_N) is the lepton (nucleon) mass. $\phi_n^2(0) = (Z\alpha)^3 m_R^3/(n^3\pi)$ is the wave function squared of the atomic $ns_{1/2}$ state at the origin, with m_R denoting the lepton-nucleus reduced mass.

*Contact author: jichen@ccnu.edu.cn

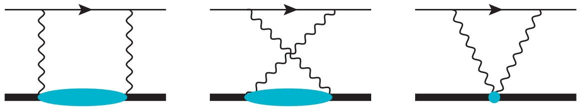

FIG. 1. Doubly virtual two-photon exchange diagrams.

Its contribution to HFS is at α^4 and is evaluated as the expectation on the atomic hyperfine state by

$$E_F = \langle (ns_{1/2}, N_0 I) F M_F | \mathcal{H}_I | (ns_{1/2}, N_0 I) F M_F \rangle, \quad (4)$$

where $|N_0 I\rangle$ is the nuclear ground state with spin I, and F and M_F denote the total angular momentum and its z projection.

The TPE effect arises at α^5, driven by doubly virtual photon exchanges between the nucleus and the lepton, as illustrated in Fig. 1. The corresponding operator is expressed in Lorenz gauge as [31]

$$\mathcal{H}_{2\gamma} = i(4\pi\alpha)^2 \phi_n^2(0) \int \frac{d^4 q}{(2\pi)^4} \frac{\eta_{\mu\nu}(q) T^{\mu\nu}(q,-q)}{(q^2+i\epsilon)^2 (q^2 - 2m_\ell q_0 + i\epsilon)}, \quad (5)$$

where η and T, respectively, represent the lepton and nuclear tensors. Only the lepton-spin-dependent part $\tilde{\eta}^{\mu\nu} = i q_0 \epsilon^{0\mu\nu i} \sigma_i^{(\ell)} + i \epsilon^{\mu\nu i j} \sigma_i^{(\ell)} q_j$ of the lepton tensor contributes to HFS. The third diagram in Fig. 1 is the nuclear seagull tensor $B_{\mu\nu}$. The charge-current part B_{0m} is of relativistic order at $1/m_N^2$. The current-current part B_{ij} gets canceled due to crossing symmetry [31,34].

TPE polarizability—We find the inelastic TPE operators by using the spin-dependent part of the lepton tensor and incorporating a summation over nuclear excitations in the nuclear tensor [31]

$$\mathcal{H}_{\rm pol}^{(0)} = \frac{i\alpha^2 \phi_n^2(0)}{2\pi m_\ell^2} \int d\omega \int \frac{d^3 q}{\boldsymbol{q}^4} h^{(0)}(\omega, |\boldsymbol{q}|) \times \boldsymbol{\sigma}^{(\ell)} \cdot \{\boldsymbol{q} \times \boldsymbol{J}(-\boldsymbol{q}), J_0(\boldsymbol{q})\} \delta(\omega - \omega_N), \quad (6)$$

$$\mathcal{H}_{\rm pol}^{(1)} = \frac{i\alpha^2 \phi_n^2(0)}{2\pi m_\ell^2} \int d\omega \int \frac{d^3 q}{\boldsymbol{q}^2} h^{(1)}(\omega, |\boldsymbol{q}|) \times \boldsymbol{\sigma}^{(\ell)} \cdot [\boldsymbol{J}(-\boldsymbol{q}) \times \boldsymbol{J}(\boldsymbol{q})] \delta(\omega - \omega_N), \quad (7)$$

where ω_N denotes the excitation energy of the nuclear state. $\mathcal{H}_{\rm pol}^{(0)}$ involves the charge-current transition matrix with the two operators in anticommutation. $\mathcal{H}_{\rm pol}^{(1)}$ involves the current-current matrix with the two currents in commutation, and is 1 order higher in $1/m_N$. The kernels $h^{(0,1)}$ are

$$h^{(0}(\omega, q) = \left[2 + \frac{\omega}{E_q}\right] \frac{E_q^2 + m_\ell^2 + E_q \omega}{(E_q + \omega)^2 - m_\ell^2} - \frac{2q + \omega}{q + \omega}, \quad (8)$$

$$h^{(1)}(\omega, q) = \frac{1}{E_q} \frac{E_q^2 + m_\ell^2 + E_q \omega}{(E_q + \omega)^2 - m_\ell^2} - \frac{1}{q + \omega}, \quad (9)$$

with $E_q = \sqrt{q^2 + m_\ell^2}$.

To obtain the polarizability corrections $E_{\rm pol}^{(0,1)}$, we replace $\mathcal{H}_{\rm I}$ with $\mathcal{H}_{\rm pol}^{(0,1)}$ in Eq. (4). Using the Wigner-Eckart theorem, we factorize the lepton and nuclear matrix elements in $E_{\rm pol}^{(0,1)}$, expressing them as ratios to E_F. We write J_0 as charge density ρ and decompose $\boldsymbol{J}$ into convection ($\boldsymbol{J}_c$) and magnetic ($\boldsymbol{J}_m$) currents. This leads to the following photo-induced nuclear sum rules:

$$E_{\rm pol}^{(0)} = \frac{6\alpha m_N E_F}{\pi m_l g_m I} \int_{\omega_{\rm th}}^{\infty} d\omega \int_0^{\infty} dq h^{(0)}(\omega, q) S^{(0)}(\omega, q), \quad (10)$$

$$E_{\rm pol}^{(1)} = -\frac{6\alpha m_N E_F}{\pi m_l g_m I} \int_{\omega_{\rm th}}^{\infty} d\omega \int_0^{\infty} dq h^{(1)}(\omega, q) S^{(1)}(\omega, q), \quad (11)$$

where $\omega_{\rm th} = (\gamma^2 + q^2/4)/m_N$ is the minimum deuteron excitation energy in the inelastic TPE. The nuclear excitations in the deuteron are represented by the scattering state $|\psi_{\boldsymbol{p}}\rangle$. The deuteron charge-magnetic ($S^{(0)}$) and convection-magnetic ($S^{(1)}$) response functions are

$$S^{(0)}(\omega, q) = \frac{m_N p}{64\pi^4 q^2} \iint d\hat{p} d\hat{q} \times {\rm Im}(\langle N_0 I I | \rho(-\boldsymbol{q}) | \psi_{\boldsymbol{p}} \rangle \langle \psi_{\boldsymbol{p}} | [\boldsymbol{q} \times \boldsymbol{J}_m(\boldsymbol{q})]_3 | N_0 I I \rangle) \quad (12)$$

$$S^{(1)}(\omega, q) = \frac{m_N p}{64\pi^4} \iint d\hat{p} d\hat{q} \epsilon^{3jk} \times {\rm Im}(\langle N_0 I I | \boldsymbol{J}_{c,j}(-\boldsymbol{q}) | \psi_{\boldsymbol{p}} \rangle \langle \psi_{\boldsymbol{p}} | \boldsymbol{J}_{m,k}(\boldsymbol{q}) | N_0 I I \rangle), \quad (13)$$

where $|N_0 I I\rangle$ denotes the nuclear ground state with spin maximally projected in the z direction. The deuteron excitation involves the NN scattering states at relative momentum $p = \sqrt{m_N \omega - \gamma^2 - q^2/4}$. The deuteron D-wave correction to $S^{(0)}$ is given by $S_{\rm sd}^{(0)}$. Its contribution to the polarizability effect, $E_{\rm pol,sd}^{(0)}$, follows the same weighted sum rule as in Eq. (10).

Elastic TPE—The elastic TPE contribution involves the insertion of the momentum-boosted nuclear ground state into the nuclear tensor $T_{\mu\nu}$, leading to

$$E_{\rm el}^{(0)} = \frac{2\alpha E_F}{\pi m_l} \int_0^{\infty} dq \left[h^{(0)}\left(\frac{q^2}{4m_N}, q\right) F_{md}(q) F_{ed}(q) - \frac{4 m_l m_R}{q^2} \right], \quad (14)$$

$$E_{\rm el}^{(1)} = -\frac{\alpha E_F}{2\pi m_l m_N}\int_0^\infty dq q^2 h^{(1)}\left(\frac{q^2}{4m_N}, q\right) F_{md}(q) F_{ed}(q), \tag{15}$$

where $q^2/(4m_N)$ is the deuteron recoil energy in the elastic TPE process. The deuteron electric and magnetic form factors, F_{ed} and F_{md} are normalized to 1 at $q = 0$. The function $h^{(0)}$ is approximated by $4m_l m_R/q^2$ when taking $m_N \gg m_l$, changing $E_{\rm el}^{(0)}$ to the pure Zemach contribution $E_{\rm zem} = -2\alpha m_R r_Z$ [25,26]. The subtraction term in Eq. (14) cancels the infrared divergence of the q integration and prevents a double counting in the iteration of the lowest-order single-photon exchange in the point-nucleus limit [35]. $E_{\rm el}^{(1)}$ is also a convolution of nuclear magnetic and electric densities but is suppressed by $1/m_N$ relative to $E_{\rm el}^{(0)}$.

A higher-order correction to $E_{\rm el}^{(0)}$ arises from the deuteron S-to-D-state mixing, and is given by

$$E_{\rm el-sd}^{(0)} = \frac{\alpha\mu_Q E_F}{3\pi m_l}\int_0^\infty dq q^2 h^{(0)}\left(\frac{q^2}{4m_N}, q\right) F_{md}(q) F_{Qd}(q), \tag{16}$$

where F_{Qd} denotes the deuteron quadrupole form factor, which is normalized to 1 at $q = 0$.

Single-nucleon TPE—Another correction to HFS arises from TPE between the lepton and a single nucleon, and includes the nucleon's Zemach, recoil, and polarizability effects. When embedded in a nucleus, the single-nucleon TPE contributions in ^{2}H and μ^2H are [28,31]

$$E_{1N} = -\frac{2\alpha m_l m_N E_F}{g_m(m_l + m_N)}(\kappa_p \tilde{r}_Z^p + \kappa_n \tilde{r}_Z^n), \tag{17}$$

where $\tilde{r}_Z^p$ and $\tilde{r}_Z^n$ represent the effective proton and neutron Zemach radii, accounting for the full single-nucleon TPE effects [36–40].

Pionless effective field theory—$\not{\pi}$EFT enables precise low-energy predictions in few-nucleon systems by embedding high-momentum effects using power counting, regularization, and renormalization. The power counting is guided by the ratio $Q = \gamma/m_\pi \approx 0.33$, with the pion mass m_π denoting the breakdown scale and the upper limit for the theory's predictive power. The order-by-order Lagrangian construction is based on the Q expansion and maintains renormalizability at each order. It incrementally refines the precision of low-energy predictions and ensures the theory's model independence. This framework has been utilized to study the TPE effects on the Lamb shift in μ^2H [41–43].

We employ the identical Lagrangian used in Ref. [41] to compute the two-nucleon bound and scattering states utilizing dimensional regularization and power-divergence subtraction renormalization. In addition, we include the NNLO S-to-D-wave mixing operator [44–46]

$$\mathcal{L}_{\rm sd} = \frac{C_0^{(\rm sd)}}{4} d_i^\dagger \left[N^T P^j \left(\overleftrightarrow{\nabla}_i \overleftrightarrow{\nabla}_j - \frac{\delta_{ij}}{3}\overleftrightarrow{\nabla}^2\right) N\right] + \text{H.c.}, \tag{18}$$

where $\overleftrightarrow{\nabla} \equiv \overleftarrow{\nabla} - \overrightarrow{\nabla}$, γ denotes the deuteron binding momentum and μ the power-divergence subtraction renormalization scale. $C_0^{(sd)} = -6\sqrt{2}\pi\eta_{sd}/[m_N\gamma^2(\mu - \gamma)]$ [44–46] matches the deuteron's asymptotic D-to-S wave ratio $\eta_{sd} = 0.0252$ [47].

P-wave contact interactions enter $\not{\pi}$EFT at N^{3}LO [48,49]. Furthermore, the relativistic correction to the kinetic term is suppressed by $\gamma^2/m_N^2 \approx Q^4$ [50], thus of N^{4}LO size. We neglect these higher-order terms in this work.

The one-nucleon current originates from minimal substitution in the free part of the Lagrangian and is [48,50]

$$\begin{aligned}\mathcal{L}_{{\rm EM},1b} = &-\frac{e}{2}N^\dagger[F_{es}(q) + \tau_3 F_{ev}(q)]N A_0 \\ &-\frac{ie}{4m_N}N^\dagger\overleftrightarrow{\nabla}[F_{es}(q) + \tau_3 F_{ev}(q)]N\cdot\boldsymbol{A} \\ &+\frac{e}{2m_N}N^\dagger[\kappa_0 F_{ms}(q) + \kappa_1\tau_3 F_{mv}(q)]\boldsymbol{\sigma}\cdot\boldsymbol{B}N,\end{aligned} \tag{19}$$

where $\boldsymbol{\sigma}$ denotes the nucleon Pauli matrices. The nucleon isoscalar and isovector anomalous magnetic factors denoted as κ_0 and κ_1 are related to the magnetic factors of the proton and neutron by $\kappa_0 = (\kappa_p + \kappa_n)/2$ and $\kappa_1 = (\kappa_p - \kappa_n)/2$. In Eq. (19), the nucleon electric and magnetic isoscalar (isovector) form factors $F_{es}(F_{ev})$ and $F_{ms}(F_{mv})$ relate to the neutron and proton electric and magnetic form factors by $F_{es(ev)} = F_{ep} \pm F_{en}$ and $\kappa_{0(1)}F_{ms(mv)} = (\kappa_p F_{mp} \pm \kappa_n F_{mn})/2$. We adopt the form factor parametrization based on dispersion analysis of the time and spacelike eN scattering data [51–53].

Two-nucleon currents appear at higher orders in $\not{\pi}$EFT. Introducing covariant derivatives in the np spin-triplet interaction gives rise to a two-nucleon convection current at NLO, whose interaction Lagrangian is

$$\mathcal{L}_{2,C} = \frac{ieC_2}{4}F_{ev}(q) d_i^\dagger (N^T \overleftrightarrow{\nabla} P_i \tau_3 N)\cdot\boldsymbol{A} + \text{H.c.}, \tag{20}$$

where C_2 represents the known coefficient of the two-nucleon NLO interaction [50]. $\mathcal{L}_{2,C}$ does not contribute to nuclear electric form factors but affects nuclear polarization. Furthermore, the two-nucleon magnetic current, which couples with the np spin-triplet interaction, emerges at NLO but not through minimal substitution,

$$\mathcal{L}_{2,B} = -ieL_2 F_{ms}(q)\epsilon_{ijk} d_i^\dagger d_j B_k + \text{H.c.}, \tag{21}$$

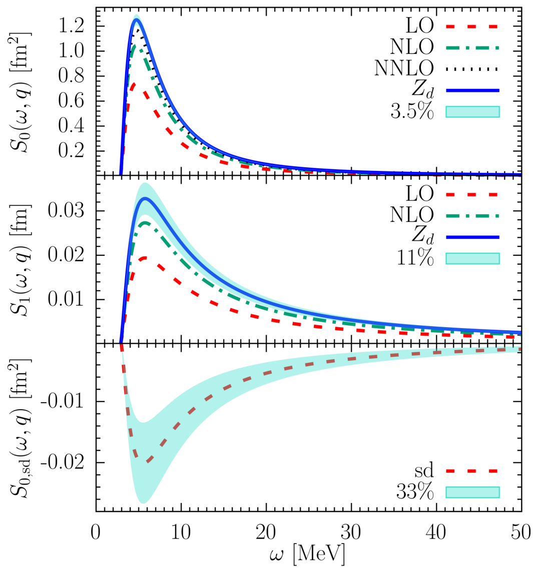

FIG. 2. The response functions $S^{(0)}$ (top panel), $S^{(1)}$ (middle panel), and $S^{(0)}_{\mathrm{sd}}$ (bottom panel) are shown as functions of ω for a fixed $q = 50$ MeV. The leading, subleading, sub-subleading, and Z_d-improved results are represented by the red dashed, green dot-dashed, black dotted, and blue solid lines, respectively. The light-blue band represents the uncertainty error from omitted higher-order corrections.

with $L_2 = (g_m - 2\kappa_0)\pi/[2m_N\gamma(\mu - \gamma)^2]$ determined by matching to the measured magnetic g factor. The two-nucleon magnetic current causes the np spin-singlet-to-triplet transition to emerge at NLO but does not contribute to TPE in HFS due to spin-parity selection rules. Other two-nucleon currents are beyond NNLO [48,50].

The transition matrices necessary for calculating the response functions in Eqs. (12) and (13) are determined using a similar approach as in Ref. [41]. The detailed expressions can be found in the Supplemental Material [54].

Results—The TPE correction to HFS consists of the elastic, polarizability, and single-nucleon contributions

$$E^{\mathrm{HFS}}_{\mathrm{TPE}} = E_{\mathrm{el}} + E_{\mathrm{pol}} + E_{1p} + E_{1n}. \tag{22}$$

The response functions in Eqs. (12) and (13) are numerically evaluated in the $\not{\pi}$EFT framework. The results are independent of ultraviolet cutoffs. This affirms that the prediction is insensitive to the short-range characteristics of the underlying theory, and thus ensures its model independence. Figure 2 displays the charge-magnetic response function $S^{(0)}$, its S-D mixing correction $S^{(0)}_{\mathrm{sd}}$, and the convection-magnetic one $S^{(1)}$, as functions of the excitation energy ω at a fixed transfer momentum $q = 50$ MeV. $S^{(0)}$, which dominates in the polarizability effect, is calculated at NNLO, while $S^{(1)}$, whose contribution is suppressed by $\gamma/m_N \approx Q^2$, is evaluated at NLO. Following Refs. [41,55,56], $S^{(0,1)}$ are Z_d-improved for better accuracy by accounting for the remaining effective range correction in the deuteron asymptotic normalization constant. A relative uncertainty of $Q^3 \approx 3.5\%$ ($Q^2 \approx 11\%$) is roughly estimated for $S^{(0)}$ [$S^{(1)}$], due to omitted N^{3}LO (NNLO) corrections. $S^{(0)}_{\mathrm{sd}}$, expected at NNLO, carries a relative uncertainty of $Q \approx 33\%$ due to its omitted subleading correction. Inserting the response functions in Eqs. (10) and (11) leads to the polarizability effects $E_{\mathrm{pol}} = E^{(0)}_{\mathrm{pol}} + E^{(1)}_{\mathrm{pol}} + E^{(0)}_{\mathrm{pol,sd}}$.

With the deuteron form factors evaluated in $\not{\pi}$EFT, the elastic TPE is a summation of contributions in Eqs. (14)–(16), $E_{\mathrm{el}} = E^{(0)}_{\mathrm{el}} + E^{(1)}_{\mathrm{el}} + E^{(0)}_{\mathrm{el,sd}}$. It is different from the Zemach contribution E_{zem} due to the additional recoil corrections in E_{el}. The prediction of r_Z from $\not{\pi}$EFT is mainly determined by the deuteron S wave, with a 3.2% correction due to S-D mixing,

$$r^D_{Z,\mathrm{th}} = 2.691\ \mathrm{fm} - 0.086\ \mathrm{fm} = 2.605(91)\ \mathrm{fm}. \tag{23}$$

The prediction has a $Q^3 = 3.5\%$ uncertainty from N^{3}LO corrections. The result is consistent with the calculation using the chiral EFT potential [57], and agrees with the experimental value $r_{Z,\mathrm{exp}} = 2.593(16)$ fm within 1σ.

The single-nucleon TPE contributions from Eq. (17) need inputs for $\tilde{r}^{p,n}_Z$, which accounts for the Zemach, recoil, and polarizability effects from proton and neutron. The proton TPE contributions to HFS in H and μH were determined with high accuracy by using constraints from HFS spectroscopy measurements [38,58], while the neutron TPE effects were determined using a dispersive calculation [36,37]. These nucleon TPE effects are transformed as follows into $\tilde{r}^{p,n}_Z$ for ordinary and muonic atoms using a scaling approach [28]:

$$\tilde{r}^{p,e}_Z = 0.883(2)\ \mathrm{fm}, \qquad \tilde{r}^{p,\mu}_Z = 0.906(2)\ \mathrm{fm},$$
$$\tilde{r}^{n,e}_Z = 0.347(38)\ \mathrm{fm}, \qquad \tilde{r}^{n,\mu}_Z = 0.102(39)\ \mathrm{fm}. \tag{24}$$

Table I summarizes the elastic, polarizability, and single-nucleon TPE effects to HFS in ^{2}H and μ^2H, comparing our predictions with measurements and other theoretical predictions. The uncertainty analysis for E_{el}, E_{pol}, and $E_{\mathrm{nucl}} = E_{\mathrm{el}} + E_{\mathrm{pol}}$ is detailed in the Supplemental Material [54]. The sources of uncertainty are categorized into the following five contributions: (i) The primary uncertainty is due to $\not{\pi}$EFT truncation at NNLO. It is analyzed with a systematic method [42], which has been shown to correspond to the Bayesian analysis [59,60]. (ii) The uncertainty from using different nucleon form factor parametrizations [51–53,61] in calculating E_{nucl} is at least 4 times smaller. (iii) The numerical uncertainty from integrations over q and ω for E_{el} and E_{pol} is 100 times less than the EFT truncation error. The total uncertainties for E_{el}, E_{pol}, and E_{nucl} are the quadrature sum of the three aforementioned uncorrelated sources. (iv) Single-nucleon TPE uncertainties are derived

TABLE I. Single-nucleon, nuclear elastic, and polarizability contributions to TPE. The subscript "mod" denotes modifications made to the findings in Refs. [30,31], incorporating nucleon recoil and polarizability effects.

	^{2}H (1S) [kHz]	μ^2H (1S) [meV]	μ^2H (2S) [meV]
$E_{\rm el}^{(0)}$	−41.2	−1.003	−0.125
$E_{\rm el}^{(1)}$	−1.95	−0.011	−0.0014
$E_{\rm el,sd}^{(0)}$	0.97	0.030	0.0037
$E_{\rm el}$	−42.1(2.1)	−0.984(46)	−0.123(6)
$E_{\rm pol}^{(0)}$	122.2	3.111	0.389
$E_{\rm pol}^{(1)}$	−7.8	−0.129	−0.016
$E_{\rm pol,sd}^{(0)}$	−4.6	−0.120	−0.015
$E_{\rm pol}$	109.8(4.5)	2.86(12)	0.358(14)
$E_{\rm nucl} = E_{\rm el} + E_{\rm pol}$	67.7(4.2)	1.878(88)	0.235(11)
$E_{1\rm p}$ [38]	−35.54(8)	−1.018(2)	−0.1272(2)
$E_{1\rm n}$ [36]	9.6(1.0)	0.079(32)	0.010(4)
$\Delta_{3\gamma}$ uncertainty	±0.49	±0.052	±0.0065
$E_{\rm TPE}$	41.7(4.4)	0.94(11)	0.117(13)
Refs. [32,33]	43		
Refs. [30,31] $_{\rm mod}$	64.5		
Ref. [28]		0.304(68)	0.0383(86)
$\nu_{\rm exp} - \nu_{\rm QED}$ [24,27]	45.2		0.0966(73)

by combining Eqs. (17) and (24). (v) We also include the uncertainty from omitted three-photon nuclear effects, $\Delta_{3\gamma}$, as detailed in [54]. The uncertainty for each contribution and the total uncertainty for $E_{\rm TPE}$ (in a quadrature sum) are shown in Table I. Our calculated TPE contribution to the ^{2}H 1S HFS is 41.7(4.4) kHz, aligning with the experimental-QED discrepancy $\nu_{\rm exp} - \nu_{\rm QED}$ (1) within 1σ of the combined theory-experiment uncertainty. The predicted TPE contribution to the μ^2H 2S HFS is 0.117(13) meV, which exceeds $\nu_{\rm exp} - \nu_{\rm QED}$ (2) by 17% but remains compatible within 1.3σ.

In comparison, the TPE effect on HFS in ^{2}H was initially calculated using the zero-range approximation [32,33], showing agreement within 5% with $\nu_{\rm exp} - \nu_{\rm QED}$ (1). This formalism was revisited in Ref. [29] to include higher-order elastic recoil corrections and was extended to estimate polarizability effects on HFS in μ^2H [27,62]. This approach introduces a 33% discrepancy in the deuteron's asymptotic behavior and an unquantified model-dependent uncertainty through an arbitrary energy-integration cutoff. Thus, their agreement with experiments may be accidental.

Alternatively, the Low-term formalism takes the heavy-nucleon-mass limit and evaluates $E_{\rm el} + E_{\rm pol}$ in closure approximation without explicitly treating nuclear excitations. However, the approximation becomes inaccurate when the momentum scale of nuclear excitations is comparable to m_l or γ, changing the infrared q dependence in Eq. (5). Their predicted TPE effect in ^{2}H was 46 kHz, whose agreement with $\nu_{\rm exp} - \nu_{\rm QED}$ (1) is accidental due to the omission of single-nucleon recoil and polarizability effects. Adding these corrections, the modified TPE prediction becomes $E_{\rm TPE}^{\rm HFS}(^2{\rm H}) = 64$ kHz, disagreeing with $\nu_{\rm exp} - \nu_{\rm QED}$ by 43%. Kalinowski *et al.* expanded the Low-term formalism with higher-order polarizability corrections to probe the TPE effect in μ^2H, and obtained $E_{\rm TPE}^{\rm HFS}(\mu^2{\rm H}) = 0.38$ meV [28], accounting for only 40% of $\nu_{\rm exp} - \nu_{\rm QED}$ (2). However, their perturbative expansion on the transition energy may overemphasize high-energy contributions to polarizability corrections, yielding a large cancellation with the Low term and possibly causing the difference with our results.

Conclusion—The N^{3}LO corrections in $\not\pi$EFT limit the accuracy of our prediction for the TPE effect on HFS. As another limiting factor, the uncertainty from the single-nucleon TPE effect may be underestimated due to the 1 order of magnitude discrepancy between the proton polarizability effects to HFS from χPT [38–40] and from dispersion analysis [36,37]. This dispute also raises questions about the predicted neutron polarizability. A resolution to the single-nucleon TPE discrepancy requires higher-order χPT calculations and future HFS measurements of the 1S state in μH [63–65]. Alternatively, one can pin down the single-nucleon effects from HFS in ^{2}H and μ^2H, where it will be crucial to improve the accuracy of calculations of the nuclear-structure part of TPE with $\not\pi$EFT beyond NNLO or with χEFT, and to measure HFS in ^{2}H and μ^2H with higher precision. Furthermore, the formalism developed in this work can also be applied to future investigations of TPE effects on HFS in other light atomic systems.

Acknowledgments—We gratefully acknowledge valuable discussions with Daniel Philips, Sonia Bacca, Thomas Richardson, and Javier Hernandez during the project. C. J. extends gratitude to Yong-Hui Lin for sharing the data on nucleon form factors. This work was supported by the National Natural Science Foundation of China (Grants No. 12175083, No. 12335002, and No. 11805078), the National Science Foundation (Grant No. PHY-2111426), and the Office of Nuclear Physics, US Department of Energy (Contract No. DE-AC05-00OR22725).

[1] R. Pohl *et al.*, Nature (London) **466**, 213 (2010).
[2] A. Antognini *et al.*, Science **339**, 417 (2013).
[3] R. Pohl *et al.*, Science **353**, 669 (2016).
[4] K. Schuhmann *et al.* (CREMA Collaboration), arXiv:2305.11679.
[5] J. J. Krauth *et al.*, Nature (London) **589**, 527 (2021).
[6] K. Pachucki, Phys. Rev. Lett. **106**, 193007 (2011).
[7] C. Ji, N. Nevo Dinur, S. Bacca, and N. Barnea, Phys. Rev. Lett. **111**, 143402 (2013).

[8] C. Ji, S. Bacca, N. Barnea, O. J. Hernandez, and N. Nevo-Dinur, J. Phys. G **45**, 093002 (2018).

[9] N. Nevo Dinur, C. Ji, S. Bacca, and N. Barnea, Phys. Lett. B **755**, 380 (2016).

[10] O. Hernandez, A. Ekström, N. N. Dinur, C. Ji, S. Bacca, and N. Barnea, Phys. Lett. B **778**, 377 (2018).

[11] B. Acharya, V. Lensky, S. Bacca, M. Gorchtein, and M. Vanderhaeghen, Phys. Rev. C **103**, 024001 (2021).

[12] C. E. Carlson, M. Gorchtein, and M. Vanderhaeghen, Phys. Rev. A **89**, 022504 (2014).

[13] C. E. Carlson, M. Gorchtein, and M. Vanderhaeghen, Phys. Rev. A **95**, 012506 (2017).

[14] H. Hellwig, R. F. C. Vessot, M. W. Levine, P. W. Zitzewitz, D. W. Allan, and D. J. Glaze, IEEE Trans. Instrum. Meas. **19**, 200 (1970).

[15] D. J. Wineland and N. F. Ramsey, Phys. Rev. A **5**, 821 (1972).

[16] S. D. Rosner and F. M. Pipkin, Phys. Rev. A **1**, 571 (1970).

[17] J. Kowalski, R. Neumann, S. Noehte, K. Scheffzek, H. Suhr, and G. z. Putlitz, Hyperfine Interact. **15**, 159 (1983).

[18] H. Guan *et al.*, Phys. Rev. A **102**, 030801(R) (2020).

[19] W. Sun *et al.*, Phys. Rev. Lett. **131**, 103002 (2023).

[20] B. Ohayon *et al.* (QUARTET Collaboration), MDPI Phys. **6**, 206 (2024).

[21] P. Strasser *et al.* (MuSEUM Collaboration), J. Phys. Conf. Ser. **2462**, 012023 (2023).

[22] C. Schwartz, Phys. Rev. **97**, 380 (1955).

[23] G. K. Woodgate, *Elementary Atomic Structure*, 2nd ed., Oxford Science Publications (Oxford University Press, London, England, 1983).

[24] M. I. Eides, H. Grotch, and V. A. Shelyuto, Phys. Rep. **342**, 63 (2001).

[25] A. C. Zemach, Phys. Rev. **104**, 1771 (1956).

[26] J. Friar and I. Sick, Phys. Lett. B **579**, 285 (2004).

[27] J. J. Krauth, M. Diepold, B. Franke, A. Antognini, F. Kottmann, and R. Pohl, Ann. Phys. (Amsterdam) **366**, 168 (2016).

[28] M. Kalinowski, K. Pachucki, and V. A. Yerokhin, Phys. Rev. A **98**, 062513 (2018).

[29] R. N. Faustov and A. P. Martynenko, Phys. Rev. A **67**, 052506 (2003).

[30] J. L. Friar and G. L. Payne, Phys. Lett. B **618**, 68 (2005).

[31] J. L. Friar and G. L. Payne, Phys. Rev. C **72**, 014002 (2005).

[32] I. B. Khriplovich, A. I. Milshtein, and S. S. Petrosian, Phys. Lett. B **366**, 13 (1996).

[33] I. B. Khriplovich and A. I. Milstein, J. Exp. Theor. Phys. **98**, 181 (2004).

[34] J. Friar and M. Rosen, Ann. Phys. (N.Y.) **87**, 289 (1974).

[35] C. E. Carlson, V. Nazaryan, and K. Griffioen, Phys. Rev. A **83**, 042509 (2011).

[36] O. Tomalak, Eur. Phys. J. A **55**, 64 (2019).

[37] O. Tomalak, Phys. Rev. D **99**, 056018 (2019).

[38] A. Antognini, F. Hagelstein, and V. Pascalutsa, Annu. Rev. Nucl. Part. Sci. **72**, 389 (2022).

[39] F. Hagelstein and V. Pascalutsa, Proc. Sci. CD15 (**2016**) 077.

[40] F. Hagelstein, Few-Body Syst. **59**, 93 (2018).

[41] S. B. Emmons, C. Ji, and L. Platter, J. Phys. G **48**, 035101 (2021).

[42] V. Lensky, F. Hagelstein, and V. Pascalutsa, Eur. Phys. J. A **58**, 224 (2022).

[43] V. Lensky, F. Hagelstein, and V. Pascalutsa, Phys. Lett. B **835**, 137500 (2022).

[44] J.-W. Chen, G. Rupak, and M. J. Savage, Phys. Lett. B **464**, 1 (1999).

[45] X.-D. Ji and Y.-C. Li, Phys. Lett. B **591**, 76 (2004).

[46] S. I. Ando and C. H. Hyun, Phys. Rev. C **72**, 014008 (2005).

[47] V. G. J. Stoks, R. A. M. Klomp, C. P. F. Terheggen, and J. J. de Swart, Phys. Rev. C **49**, 2950 (1994).

[48] G. Rupak, Nucl. Phys. **A678**, 405 (2000).

[49] J.-W. Chen and M. J. Savage, Phys. Rev. C **60**, 065205 (1999).

[50] J.-W. Chen, G. Rupak, and M. J. Savage, Nucl. Phys. **A653**, 386 (1999).

[51] Y.-H. Lin, H.-W. Hammer, and U.-G. Meißner, Eur. Phys. J. A **57**, 255 (2021).

[52] Y.-H. Lin, H.-W. Hammer, and U.-G. Meißner, Phys. Lett. B **816**, 136254 (2021).

[53] Y.-H. Lin, H.-W. Hammer, and U.-G. Meißner, Phys. Rev. Lett. **128**, 052002 (2022).

[54] See Supplemental Material at http://link.aps.org/supplemental/10.1103/PhysRevLett.133.042502 for the TPE formalism derived in $\not\pi$EFT and a detailed uncertainty quantification of the resulting calculations.

[55] D. R. Phillips, G. Rupak, and M. J. Savage, Phys. Lett. B **473**, 209 (2000).

[56] D. R. Phillips and T. D. Cohen, Nucl. Phys. **A668**, 45 (2000).

[57] N. Nevo Dinur, O. J. Hernandez, S. Bacca, N. Barnea, C. Ji, S. Pastore, M. Piarulli, and R. B. Wiringa, Phys. Rev. C **99**, 034004 (2019).

[58] A. Antognini, Y.-H. Lin, and U.-G. Meißner, Phys. Lett. B **835**, 137575 (2022).

[59] R. J. Furnstahl, N. Klco, D. R. Phillips, and S. Wesolowski, Phys. Rev. C **92**, 024005 (2015).

[60] E. Epelbaum, H. Krebs, and U. G. Meißner, Eur. Phys. J. A **51**, 53 (2015).

[61] J. J. Kelly, Phys. Rev. C **70**, 068202 (2004).

[62] R. N. Faustov, A. P. Martynenko, G. A. Martynenko, and V. V. Sorokin, Phys. Rev. A **90**, 012520 (2014).

[63] M. Sato *et al.*, J. Phys. Soc. Jpn. Conf. Proc. **8**, 025005 (2015).

[64] C. Pizzolotto *et al.*, Eur. Phys. J. A **56**, 185 (2020).

[65] P. Amaro *et al.*, SciPost Phys. **13**, 020 (2022).